Autism Research

RESEARCH ARTICLE

Synaptic Deficits in *Adnp*-Mutant Mice Are Ameliorated by Histone Demethylase LSD1 Inhibition

Chih-Hung Lin | Yong Ren | Kin Wai Tam | Megan Conrow-Graham | Zhen Yan

Department of Physiology and Biophysics, Jacobs School of Medicine and Biomedical Sciences, State University of New York at Buffalo, Buffalo, New York, USA

Correspondence: Zhen Yan (zhenyan@buffalo.edu)

Received: 17 April 2025 | **Revised:** 17 April 2025 | **Accepted:** 9 June 2025

Funding: This work was supported by National Institutes of Health (Grants NS127728 and MH126443).

ABSTRACT

ADNP (Activity-dependent neuroprotective protein) is a top-ranking autism risk gene. Here we examined synaptic alterations in heterozygous mice carrying an autism mutation on *Adnp* C-terminus (*Adnp*^{mut}). We found that PFC pyramidal neurons in *Adnp*^{mut} mice exhibited significantly diminished glutamatergic and GABAergic synaptic transmission, as indicated by markedly reduced excitatory postsynaptic currents (EPSC) and inhibitory postsynaptic currents (IPSC). Given the key role of ADNP in chromatin regulation and the constitutive association of the ADNP complex with lysine-specific demethylase 1 (LSD1), we examined the therapeutic effects of LSD1 inhibition in *Adnp*^{mut} mice. We found that treatment with an LSD1 inhibitor significantly elevated EPSC and IPSC in PFC pyramidal neurons of *Adnp*^{mut} mice, and the rescuing effect was particularly prominent in females. Biochemical assays revealed increased H3K4me2 and decreased H3K9me2/3 by LSD1 inhibitor treatment in female *Adnp*^{mut} mice, which were correlated with the elevated expression of synaptic genes linked to glutamatergic and GABAergic transmission after the treatment. These data have revealed synaptic deficits in PFC induced by a loss-of-function mutation of *Adnp* and uncovered the therapeutic potential of LSD1 inhibition in ADNP-deficient conditions, especially for females.

1 | Introduction

ADNP, which encodes the activity-dependent neuroprotective protein (ADNP), is one of the top-ranking autism risk genes (De Rubeis et al. 2014; Satterstrom et al. 2020). Since its first discovery decades ago (Bassan et al. 1999), ADNP is found to play a multifunctional role in the nucleus and the cytoplasm (D'Incal et al. 2023; Gozes 2016). In the nucleus, ADNP acts as a chromatin regulator by interacting with a variety of chromatin remodelers (D'Incal et al. 2023). The C-terminus of ADNP interacts with the SWI/SNF complex to affect gene expression (Mandel and Gozes 2007). ADNP also binds to CHD4 and HP1γ at N- and C-termini respectively to form ChAHP complex to control lineage-specifying genes during early development and regulate chromatin looping by competing with CTCF (Kaaij et al. 2019; Ostapcuk et al. 2018). The C-terminus of ADNP also interacts with BRG1 to establish ADNP-BRG1-CHD4 (ABC-triplex) to modulate chromatin architecture (Sun et al. 2020). Moreover, ADNP forms a nuclear complex and co-occupies loci with another high-ranking autism risk factor POGZ, which promotes the transcription of clustered synaptic genes (Markenscoff-Papadimitriou et al. 2021). In the cytoplasm, ADNP acts as a translational regulator, autophagy operator, and synaptic modulator (Gozes 2016). ADNP directly interacts with the eukaryotic translation initiation factor 4E (eIF4E) to affect the protein translation machinery (Malishkevich et al. 2015). ADNP is also involved in modulating dendritic plasticity via interacting with the microtubule end-binding protein (EB) (Oz et al. 2014).

Mice with *Adnp* deficiency or loss-of-function mutations show deficits in molecular, synaptic, morphological, and behavioral measurements (Cho et al. 2023; Conrow-Graham et al. 2022; Hacohen-Kleiman et al. 2018; Karmon et al. 2022). The shRNA-based *Adnp* knockdown induced the decreased expression of synaptic genes, such as *Snap25* and *Nrxn1*, and the increased

Summary

- In mice carrying an autism mutation on the risk gene *Adnp* (*Adnp*^{mut}), the excitatory and inhibitory synaptic signals in cortical neurons were significantly diminished.
- Treatment with a pharmacologic agent that specifically inhibits the epigenetic enzyme lysine specific demethylase 1 (LSD1) significantly rescued the physiological function and synaptic gene expression in *Adnp*^{mut} mice, particularly in females.
- This study has uncovered a novel treatment strategy for autism linked to ADNP deficiency.

expression of proinflammatory genes, such as complement and cytokines (Conrow-Graham et al. 2022; Wan et al. 2024). *Adnp* haploinsufficiency models exhibited reduced spine density in cortical and hippocampal neurons (Hacohen-Kleiman et al. 2018; Karmon et al. 2022), excessive long-term potentiation, and hyperphosphorylated CaMKIIα (Cho et al. 2023), as well as anxiety-like behavior, social deficits, repetitive behaviors, and cognitive deficits (Cho et al. 2023; Conrow-Graham et al. 2022; Hacohen-Kleiman et al. 2018; Karmon et al. 2022), reminiscent of behavioral phenotypes of patients with *ADNP* mutations (Helsmoortel et al. 2014; Van Dijck et al. 2019).

Synaptic transmission in prefrontal cortical neurons is critical for cognitive and emotional processes (Yan and Rein 2022). Dysregulation of synaptic function in the frontal cortex is perceived as a convergent mechanism of autism spectrum disorders (ASD) (Delorme et al. 2013; Spooren et al. 2012). Thus, we examined the alteration of excitatory and inhibitory synaptic transmission in PFC pyramidal neurons from a mouse model harboring a patient-specific C-terminal *ADNP* mutation.

Currently, there is no therapeutic avenue for core symptoms of ASD in general and ADNP syndrome in particular. One emerging therapeutic strategy is to target epigenetic enzymes, which could potentially lead to the normalization of gene expression, synaptic function, and behavioral performance (Qin et al. 2018; Rapanelli et al. 2022; Wang et al. 2020; Yan 2024). ChAHP complex constitutively associates with the epigenetic corepressor lysine-specific histone demethylase 1A (LSD1) (Barnes et al. 2022). Inhibiting LSD1 improved symptoms in various mouse models for autism and schizophrenia (Baba et al. 2021; López-Tobón et al. 2023; Mukai et al. 2019; Rapanelli et al. 2022). Increasing LSD1 led to dampened glutamatergic transmission (Longaretti et al. 2020), suggesting LSD1 as a negative modulator of the glutamatergic synapse. In this study, we explored the therapeutic potential of treatment with an LSD1 inhibitor in rescuing *Adnp* mutation-induced synaptic deficits.

2 | Methods

2.1 | Animals and Compounds

The protocol and procedures employed were ethically reviewed and approved by the Institutional Animal Care and Use Committee (IACUC) of the State University of New York (SUNY) at Buffalo. We follow the US National Research Council's Guide for the Care and Use of Laboratory Animals, the US Public Health Service's Policy on Use of Laboratory Animals, and Guide for the Care and Use of Laboratory Animals.

Wild-type (WT) mice and *Adnp*^{mut} mice (carrying a 14-nucleotide deletion in the C-terminus, Strain # 033128, Jackson Lab) with C57BL/6J background were utilized. All mice were group-housed with food and water *ad libitum* under the regulated conditions of temperature (22°C), humidity (56%), and a 12/12 h light/dark cycle. Mice used in experiments were 2–4 months old.

GSK-LSD1 (Tocris, Cat. # 5361) was dissolved in water as a stock solution, aliquoted, and stored at −20°*C*. *Prior* to the injection, the stock solution was diluted with sterile saline as a working solution. Mice were injected with GSK-LSD1 (5 mg/kg, i.p.) or sterile saline (vehicle control) once daily for 3 days. Animals were used for experiments at 1–14 days post-injection (average post-injection duration: ~4 days).

2.2 | Electrophysiological Recordings

Whole-cell voltage-clamp recordings were performed to measure synaptic currents in layer V pyramidal neurons of the medial prefrontal cortex (mPFC) as previously described (Conrow-Graham et al. 2022; Duffney et al. 2015; Qin et al. 2018, 2021; Rapanelli et al. 2022). Mice were decapitated by guillotine under isoflurane anesthesia. Brains were promptly collected and placed in an ice-cold sucrose solution (in mM: 234 sucrose, 15 HEPES, 11 glucose, 4 $MgSO_4$, 2.5 KCl, 1 Na_2HPO_4, 0.1 $CaCl_2$, pH 7.35, 300 mOsm), and then cut into 300 μm coronal slices via a vibratome (Leica VT1000). Brain slices were incubated at 32°C in oxygenated (95% O_2 / 5% CO_2) artificial cerebrospinal fluid (aCSF) (in mM: 130 NaCl, 26 $NaHCO_3$, 10 glucose, 3.5 KCl, 1.25 NaH_2PO_4, 1 $CaCl_2$, 0.5 $MgCl_2$, pH 7.4, 300 mOsm) for 1 h for recovery and then at room temperature (22°C–24°C). After recovery, the brain slice was positioned in a perfusion chamber of the fixed stage of an upright microscope (Olympus BX51WI) submerged in continuously flowing oxygenated aCSF. Layer V PFC pyramidal neurons were visualized with a 40X water-immersion lens and recorded with the Multiclamp 700A amplifier, Digidata 1322A data acquisition system, and Clampex software (Molecular Devices, Sunnyvale, CA). Recording electrodes were pulled from borosilicate glass capillaries (1.5/0.86 mm OD/ID) with a micropipette puller (Model P-97, Sutter Instrument Co., Novato, CA). The resistance of the patch electrode was 2–4 MΩ. The threshold value of the series resistance was 25 MΩ. Evoked synaptic currents were induced with pulses by a S48 pulse generator (Grass Technologies, West Warwick, RI). A bipolar stimulating electrode (FHC, Bowdoinham, ME) was positioned ~100 μm away from the recording neuron.

To record excitatory synaptic currents, PFC neurons were held at −70 mV. To record inhibitory synaptic currents, PFC neurons were held at 0 mV. Recording pipettes were filled with the internal solution (in mM: 130 Cs-methanesulfonate, 10 CsCl, 10 HEPES, 5 EGTA, 4 NaCl, 1 $MgCl_2$, 16 phosphocreatine, 5 MgATP, 0.5 Na_2GTP, 2 QX-314, pH 7.3, 270 mOsm). Electrical

pulses (0.058 ms, 100 μA) from a stimulation isolation unit controlled by an S48 pulse generator were delivered to the neuron to record evoked synaptic currents.

2.3 | Quantitative RT-PCR

Mice were sacrificed by decapitation, brains were quickly removed and cooled on ice, and then mPFC was dissected (~20 mg each side) with sharp needles. Total RNA was isolated from the PFC region of mouse brains using Trizol reagent (Invitrogen). cDNA was synthesized from 1 μg total RNA using iScript cDNA synthesis Kit (Bio-Rad, 1,708,890). Quantitative real-time PCR was carried out using the CFX Connector RealTime System and iQ SYBR Green Supermix (Bio-Rad, 1,808,880) according to the manufacturer's instructions. In brief, *GAPDH* was used as the housekeeping gene for quantitation of the expression of target genes in each sample. Fold changes in the target genes were determined by: Fold change $= 2^{-\Delta(\Delta CT)}$, where $\Delta CT = C_T(\text{target}) - C_T(\text{GAPDH})$, and $\Delta(\Delta C_T) = \Delta CT(\text{target}) - \Delta CT(\text{control})$. The threshold cycle is defined as the fractional cycle number at which the fluorescence reaches 10x of the standard deviation of the baseline. A total reaction mixture of 20 μL was amplified in a 96-well thin-wall PCR plate (Bio-Rad, HSP9601) using the following PCR cycling parameters: 95 °C for 3 min followed by 40 cycles of 95 °C for 15 s, 60 °C for 30 s, and 72 °C for 60 s. Primers used are listed as follows:

Gene	F (5′ -> 3′)	R (5′ -> 3′)
Gapdh	AGGTCGGTGTGAACGGATTTG	TGTAGACCATGTAGTTGAGGTCA
Adnp-NT	TGCACAGGGTTGCACTTTT	AGTCCAAAGAGCAAGGCAGG
Adnp-CT	AAGAGTGACATTGCCTCCCA	AAACCTAGCAGCACACCAGG
Nrxn1	CAGCACAGCTAGAAGAGGCA	TCCTCATCGTCACTGGGACA
Nrxn3	TAGCCACAACCTCCAGGGAT	GTCCTTTGCTGGAGTTACAGTT
SYP	CCTAGTTGGTGACTACTCCT	GTTGTTCTCTCGGTACTTGT
Gria1	GCCTTAATCGAGTTCTGCTA	GAATGGATTGCATGGACTTG
Gria2	AGCCTATGAGATCTGGATGT	GAGAGAGATCTTGGCGAAAT
Gria3	TCAGCATAGGTGGACTTTTC	GTAGTTCAAATGGAAGGGCT
Gad1	GAGACACCCTGAAGTACGGG	TCGATGTCAGCCATTCACCA
Gad2	TGGGAATTGGCAGACCAACC	ACCAGTCTGCTGCTAATCCA
Gabrg3	CCGGAGCAAGTAGAGACCAAG	TACCCTCCTGGACCGAGCAT

2.4 | Western Blot

PFC was collected and homogenized on ice for 3–4 min in hypotonic buffer (20 mM Tris–HCl, 10 mM NaCl, 3 mM $MgCl_2$, 0.5% NP40, 250 μL buffer per 50 mg tissue) supplemented with 1 mM PMSF and protease inhibitor cocktail. The homogenates were incubated on ice for 15 min and then centrifuged at 1000 x g at 4°C for 10 min. The pellet containing the nuclear fraction was resuspended in 100–150 μL hypotonic buffer with 1% SDS. Protein concentration was measured with bicinchoninic acid assay (Thermo Scientific, 23,227). Samples were mixed with 4X SDS loading buffer and boiled for 5 min. Proteins were separated with 12% SDS-PAGE and subsequently transferred to PVDF membranes. The membranes were blocked with 5% non-fat milk TBS-T (50 mM Tris–HCl pH 7.4, 150 mM NaCl, 0.1% Tween 20) and then incubated with primary antibodies (anti-histone H3 (Cell Signaling, 4499S, 1:1000), anti-H3K9ac (Cell Signaling, 9649S, 1:1000), anti-H3K4me2 (Cell Signaling, 9725S, 1:1000), anti-H3K9me2 (Cell Signaling, 4658S, 1:1000), anti-H3K9me3 (Invitrogen, PA5-31910, 1:1000), anti-Adnp (C-terminus, Invitrogen, PA5-52286, 1:1000), anti-Adnp (N-terminus, Santa Cruz, sc-393,377, 1:500)), followed by probing with HRP-conjugated secondary antibodies (goat anti-mouse IgG, Invitrogen, G21040, 1:5000 or goat anti-rabbit IgG, Invitrogen, PA5-114542, 1:5000). Immunoblots were visualized using SuperSignal West Femto Maximum Sensitivity Substrate (Thermo Scientific, 34,095) and imaged with ChemiDoc (Bio-rad). The intensities of the bands were measured with ImageJ, and relative intensities were calculated using the corresponding H3 bands as references.

2.5 | Statistics

All data were analyzed by Clampfit (Molecular Devices, Sunnyvale, CA), MiniAnalysis (Synaptosoft, NJ), and GraphPad Prism (GraphPad). Experimental differences between two groups were compared with Student's *t* tests. To compare more than two groups, we used one-way ANOVA, followed by Tukey's multiple comparisons. Data were presented as mean ± SEM.

3 | Results

3.1 | *Adnp*^{mut} mice Show the Deficiency of Full-Length Adnp Expression

To find out the potential impact of *ADNP* haploinsufficiency on synaptic function, we used the heterozygous mice carrying C-terminal mutated *Adnp* (*Adnp*^{mut}). This CRISPR/Cas9

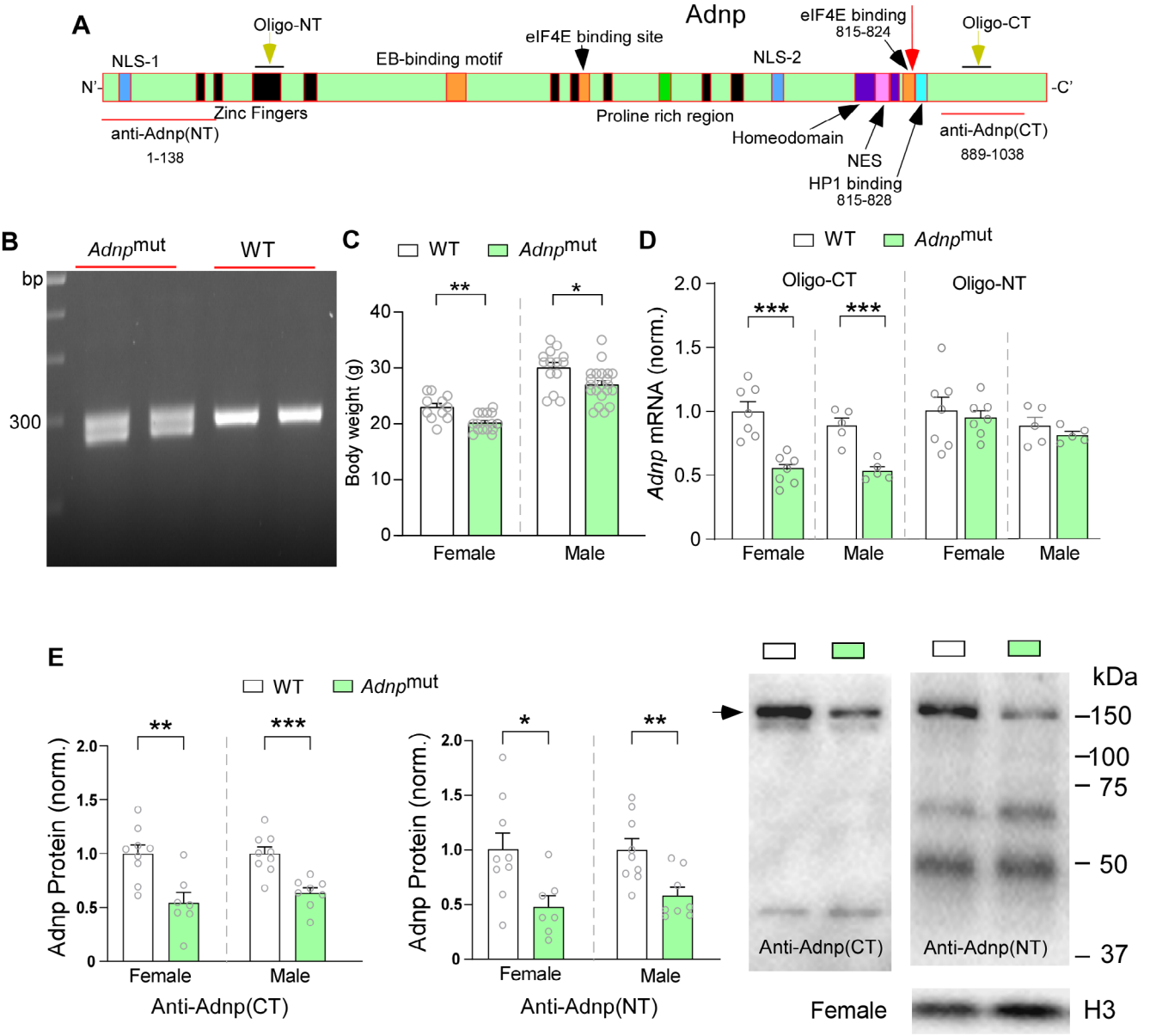

FIGURE 1 | *Adnp* mutant (*Adnp*^{mut}) mice show the reduced expression of full-length Adnp. (A) A schematic representation of functional domains along full-length mouse Adnp protein (MGI:1338758), including Zinc fingers, NLS1,2 (nuclear localization signal); Eb (microtubule plus-end binding); eIF4 (eukaryotic initiation factor 4E); HP1α (heterochromatin protein α); NES-1 (nuclear export signal). Also labeled is the mutation site of the *Adnp*^{mut} mice (red arrow), which is a 14-nucleotide deletion at C-terminus of *Adnp* on exon 5. (B) DNA gel electrophoresis of *Adnp* PCR genotyping of WT (292 kb) and heterozygous *Adnp*^{mut} mice (292/278 kb). Genotyping primers used are as follows: GAGTGACATTGCCTCCCATT (forward) and GTCAAAAGGACTCCCGCTTC (reverse). (C) Bar graphs of body weight in WT and *Adnp*^{mut} mice. (D) Quantitative PCR of *Adnp* mRNA levels detected with C-terminal (CT) or N-terminal (NT) *Adnp* oligos in WT and heterozygous *Adnp*^{mut} mice (both females and males). The positions of these oligos are labeled on A. (E) Bar graphs of immunoblot analysis on the protein level of full-length Adnp in nucleus faction using antibodies against N-terminus or C-terminus of Adnp. Inset: Representative Western blots. All data are shown as mean ± SEM. *$p < 0.05$, **$p < 0.01$, ***$p < 0.001$, *t* test.

generated mutant of the *Adnp* gene introduced a 14-nucleotide deletion, so Leucine822 was replaced by Histidine and followed by 6 amino acids and a termination codon in exon 5, which caused a frameshift and resulted in a truncated protein (Figure 1A,B). A modest but significant reduction of body weight was found in *Adnp*^{mut} mice (Figure 1C, $n = 11$–21 mice per group; females: 12.2% reduction, $t_{17} = 3.5$, $p = 0.0025$; males: 10.0% reduction, $t_{26} = 2.6$, $p = 0.016$, *t* test). Using primers against the C-terminal region of Adnp downstream of the mutation site, we found a ~50% reduction of *Adnp* mRNA in both female and male heterozygous *Adnp*^{mut} mice, compared to WT mice (Figure 1D, females, WT: $n = 7$, *Adnp*^{mut}: $n = 7$, $p < 0.001$; males, WT: $n = 5$, *Adnp*^{mut}: $n = 5$, $p < 0.001$, *t* test). In contrast, no change was found in *Adnp* mRNA when detecting with N-terminal primers (females, $p = 0.70$; males, $p = 0.44$, *t* test). It suggests that *Adnp*^{mut} mice have a significant deficiency in full-length *Adnp*.

To further check the alteration of Adnp protein in *Adnp*^{mut} mice, we performed Western blot assays in the nuclear fraction. As expected, we observed a ~50% decrease of full-length Adnp protein (~150 KDa) using anti-Adnp (C-terminus) in both female

and male *Adnp*^{mut} mice due to the heterozygous truncation at the C-terminus (Figure 1E, females, WT: $n=9$, *Adnp*^{mut}: $n=7$, $p=0.003$; males, WT: $n=9$, *Adnp*^{mut}: $n=8$, $p=0.0004$, *t* test). A similar ~50% decrease of full-length Adnp protein was also noted using anti-Adnp (N-terminus) (Figure 1E, females, $p=0.02$; males, $p=0.006$, *t* test), which could result from a decrease in the amount of full-length Adnp protein translocated to the nucleus.

3.2 | *Adnp*^{mut} Mice Exhibit Diminished Excitatory and Inhibitory Synaptic Transmission in PFC Pyramidal Neurons

Using whole-cell patch clamp recordings, we compared glutamatergic synaptic currents in layer V PFC pyramidal neurons from WT vs. *Adnp*^{mut} mice. Females and males were analyzed separately to find out whether there were sex-specific differences. As shown in Figure 2A,C, the frequency of spontaneous excitatory postsynaptic currents (sEPSC) was significantly decreased in both sexes of *Adnp*^{mut} mice ($n=7$–13 cells / 3–7 mice per group; females: 49.6% reduction, $t_{15}=2.2$, $p=0.046$; males: 44.6% reduction, $t_{17}=2.3$, $p=0.033$; All: 48.5% reduction, $t_{33}=3.0$, $p=0.0048$, *t* test). For sEPSC amplitudes, only *Adnp*^{mut} female mice had a modest reduction compared to WT females (Figure 2B, 18.0% reduction, $t_{15}=2.5$, $p=0.023$, *t* test).

To further investigate *Adnp* mutation-induced alterations of synaptic transmission, we recorded AMPAR-mediated EPSC evoked by electrical stimulations (eEPSC). As shown in Figure 2D,E, both female and male *Adnp*^{mut} mice had significantly reduced eEPSC amplitudes ($n=10$–11 cells / 3–6 mice per group; females: 64.4% reduction, $t_{16}=3.7$, $p=0.0019$; males: 47.4% reduction, $t_{18}=2.5$, $p=0.022$; All: 57.3% reduction, $t_{35}=4.4$, $p<0.001$, *t* test).

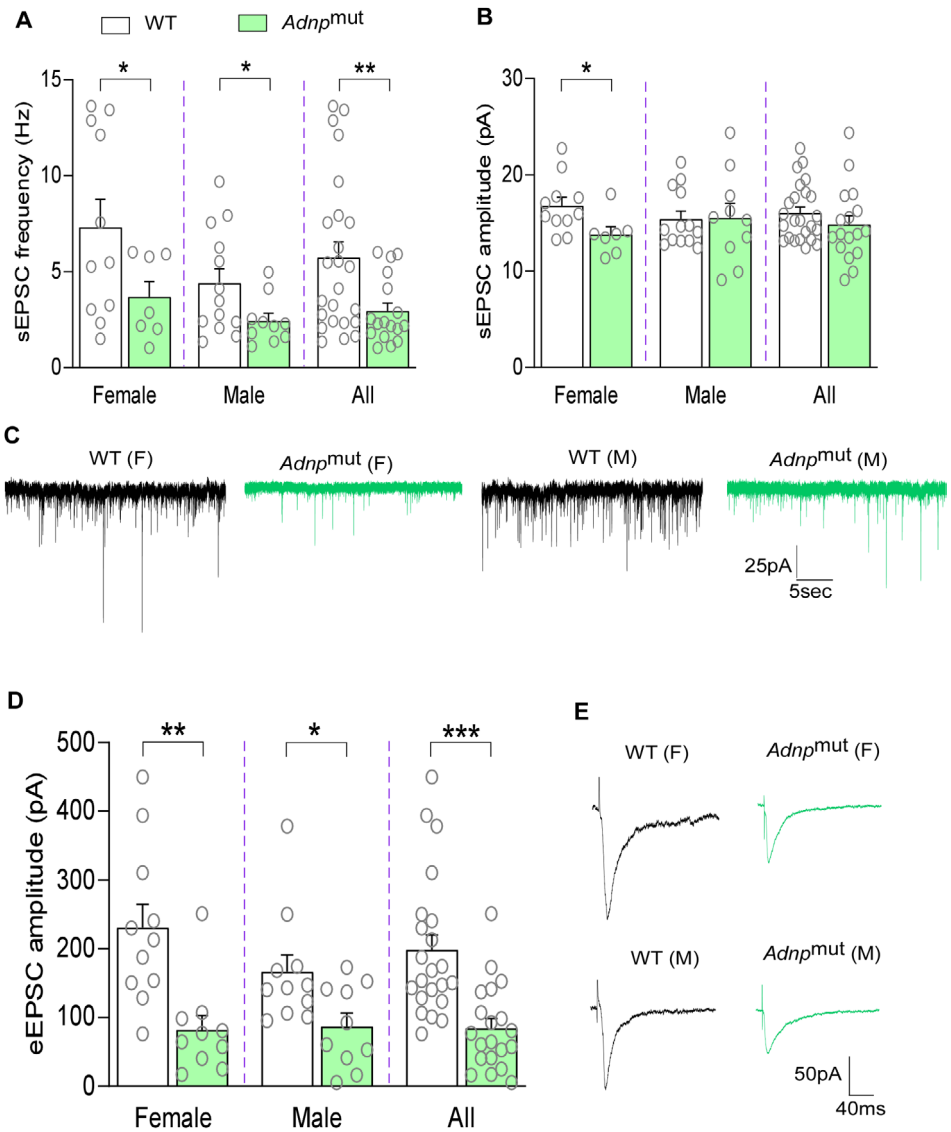

FIGURE 2 | *Adnp*^{mut} mice exhibit diminished synaptic excitation in PFC pyramidal neurons. (A, B) Bar graphs of sEPSC frequency (A) or amplitude (B) in PFC pyramidal neurons from female or male WT vs. *Adnp*^{mut} mice. (C) Representative sEPSC traces. (D) Bar graphs of eEPSC amplitude in PFC pyramidal neurons from female or male WT vs. *Adnp*^{mut} mice. (E) Representative eEPSC traces. All data are shown as mean ± SEM, $^{*}p<0.05$, $^{**}p<0.01$, $^{***}p<0.001$, *t* test.

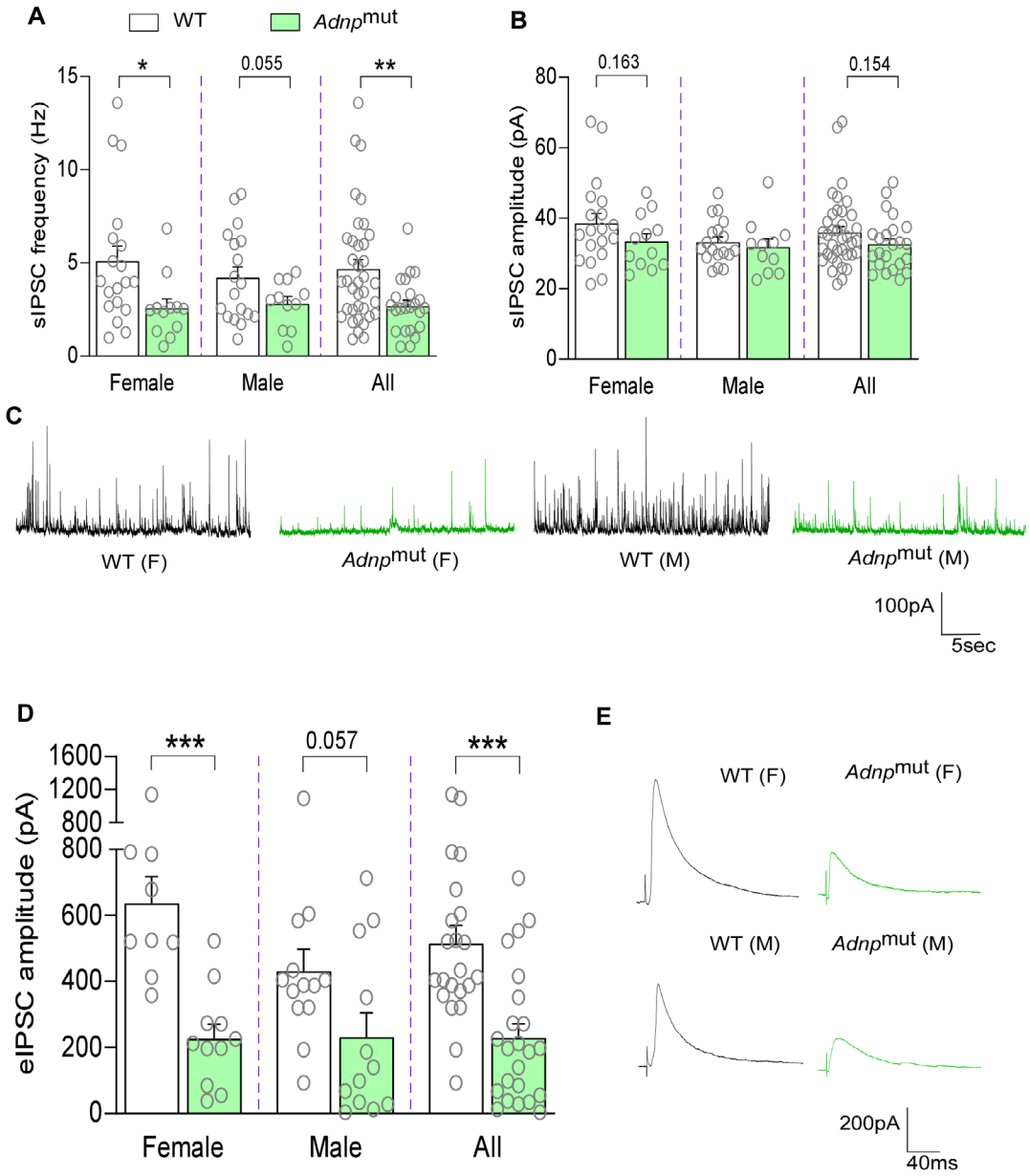

FIGURE 3 | *Adnp*^{mut} mice exhibit weakened synaptic inhibition in PFC pyramidal neurons. (A, B) Bar graphs of sIPSC frequency (A) or amplitude (B) in PFC pyramidal neurons from female or male WT vs. *Adnp*^{mut} mice. (C) Representative sIPSC traces. (D) Bar graphs of eIPSC amplitude in PFC pyramidal neurons from female or male WT vs. *Adnp*^{mut} mice. (E) Representative eIPSC traces. All data are shown as mean ± SEM, $^{*}p < 0.05$, $^{**}p < 0.01$, $^{***}p < 0.001$, *t* test.

Besides excitatory synaptic transmission, inhibitory synaptic transmission is critical for synaptic balance, which could also be affected by *Adnp* mutation (Cho et al. 2023). Hence, we performed whole-cell patch clamp recordings of GABAergic synaptic currents on layer V PFC pyramidal neurons. As shown in Figure 3A,C, the frequency of spontaneous inhibitory postsynaptic currents (sIPSC) was markedly reduced in both female and male *Adnp*^{mut} mice ($n = 11–19$ cells / 3–7 mice per group; females: 49.5% reduction, $t_{27} = 2.7$, $p = 0.013$; males: 33.1% reduction, $t_{27} = 2.0$, $p = 0.055$; All: 42.4% reduction, $t_{55} = 3.4$, $p = 0.0014$, *t* test). The amplitude of sIPSC was not significantly changed in *Adnp*^{mut} mice (Figure 3B, females: $t_{29} = 1.4$, $p = 0.16$; males: $t_{18} = 0.5$, $p = 0.62$; All: $t_{56} = 1.4$, $p = 0.15$, *t* test).

Next, we measured $GABA_A$R-mediated IPSC evoked by electrical simulations (eIPSC). As shown in Figure 3D,E, female *Adnp*^{mut} mice had significantly reduced eIPSC amplitudes, while male *Adnp*^{mut} mice also showed a strong trend of reduction of eIPSC ($n = 9–13$ cells / 3–6 mice per group; females: 64.4% reduction, $t_{13} = 4.5$, $p < 0.001$; males: 46.3% reduction, $t_{23} = 2.0$, $p = 0.057$; All: 55.5% reduction, $t_{40} = 4.1$, $p < 0.001$, *t* test).

Taken together, these electrophysiological data show that the *Adnp* mutation has led to diminished synaptic excitation and inhibition in PFC pyramidal neurons, which may directly impair PFC function.

3.3 | Treatment with an LSD1 inhibitor markedly elevates excitatory and inhibitory synaptic transmission in *Adnp*^{mut} mice, especially in Females

As ADNP is a key chromatin regulator (Kaaij et al. 2019; Ostapcuk et al. 2018), one potential mechanism underlying the physiological deficits in *Adnp*^{mut} mice is epigenetic aberration. To find out a therapeutic avenue to rescue the diminished PFC synaptic function in *Adnp*^{mut} mice, we targeted LSD1, an epigenetic enzyme associated with the ADNP complex (Barnes et al. 2022). Targeting LSD1 showed promising effects in several mouse models for neurodevelopmental disorders (Baba et al. 2021; Mukai et al. 2019; Rapanelli et al. 2022; Yan 2024). We gave *Adnp*^{mut} mice a short treatment with the LSD1 inhibitor (GSK-LSD1, 5 mg/kg, i.p., once daily for 3 days), followed by electrophysiological recordings of PFC pyramidal neurons.

As shown in Figure 4A,B, the frequency and amplitude of sEPSC were significantly elevated in LSD1 inhibitor-treated female *Adnp*^{mut} mice, while a trend of enhancement was observed in male *Adnp*^{mut} mice treated with GSK-LSD1 ($n = 11$–19 cells / 3–5 mice per group; Freq., females: 161.1% increase, $t_{27} = 4.2$, $p = 0.0002$; males: 53.9% increase, $t_{17} = 1.5$, $p = 0.16$; Amp., females: 24.1% increase, $t_{25} = 2.9$, $p = 0.007$; males:, 21.8% increase, $t_{19} = 1.7$, $p = 0.10$, *t* test). We further examined the effect of LSD1 inhibition on evoked AMPAR-EPSC. As shown in Figure 4C,D, eEPSC amplitudes were markedly elevated in LSD1 inhibitor-treated female *Adnp*^{mut} mice, while the potentiating effect of GSK-LSD1 on eEPSC was modest in male *Adnp*^{mut} mice ($n = 11$–25 cells / 3–5 mice per group; females: 283.5% increase, $t_{35} = 4.4$, $p < 0.001$; males: 38.9% increase, $t_{27} = 1.0$, $p = 0.33$, *t* test). Female or male WT mice treated with GSK-LSD1 had no significant changes in sEPSC frequency and amplitude or eEPSC amplitude (Figure 4E–H, WT + LSD1i: $n = 14$–18 cells per group from 4 females and 4 males, WT + saline, $n = 7$–10 cells per group from 2 females and 2 males. All $p > 0.05$, *t* test).

With the dramatic reduction of inhibitory transmission in PFC pyramidal neurons from *Adnp*^{mut} mice, we also examined the effect of LSD1 inhibition on GABAergic synaptic currents. As shown in Figure 5A,B, LSD1 inhibitor-treated female *Adnp*^{mut} mice showed the significantly elevated sIPSC frequency and amplitude, while LSD1 inhibitor-treated male *Adnp*^{mut} mice had a trend of enhancement of sIPSC frequency ($n = 13$–22 cells / 3–5 mice per group; Freq., females: 77.9% increase, $t_{32} = 3.4$, $p = 0.002$; males: 38.9% increase, $t_{22} = 1.5$, $p = 0.14$; Amp., females: 17.5% increase, $t_{27} = 2.0$, $p = 0.056$, t-test). Similarly, LSD1 inhibitor dramatically elevated eIPSC amplitude in female *Adnp*^{mut} mice, and only exhibited a trend of increase of eIPSC in male *Adnp*^{mut} mice (Figure 5C,D, $n = 11$–23 cells / 3–5 mice per group; females: 186.4% increase, $t_{35} = 3.8$, $p < 0.001$; males: 54.5% increase, $t_{23} = 1.1$, $p = 0.26$, *t* test). In female or male WT mice, GSK-LSD1 treatment did not induce significant changes in sIPSC frequency and amplitude or eIPSC amplitude (Figure 5E–H, WT + LSD1i: $n = 14$–18 cells per group from 4 females and 4 males, WT + saline, $n = 7$–10 cells per group from 2 females and 2 males. All $p > 0.05$, *t* test).

Taken together, these data indicate that LSD1 inhibition exerts a powerful rescuing effect on excitatory and inhibitory synaptic transmission in PFC pyramidal neurons from the *Adnp*^{mut} mice, particularly in females.

3.4 | LSD1 Inhibitor Alters Histone Modification and Synaptic Gene Expression in *Adnp*^{mut} Mice, Especially in Females

To find out the molecular basis that may underlie the diminished synaptic function in PFC pyramidal neurons of *Adnp*^{mut} mice and the rescuing effect of GSK-LSD1, we performed Western blotting and quantitative PCR to examine changes in histone marks and synaptic gene transcription by *Adnp* mutation and GSK-LSD1 treatment (5 mg/kg, i.p., once daily for 3 days).

As shown in Figure 6A, GSK-LSD1 significantly elevated the H3K4me2 level in female *Adnp*^{mut} mice (females, WT + sal: $n = 9$, *Adnp*^{mut} + sal: $n = 7$, *Adnp*^{mut} + LSD1i: $n = 11$, $F_{2,24} = 10.0$, $p < 0.001$, one-way ANOVA). While GSK-LSD1 did not change the H3K9ac level in female *Adnp*^{mut} mice, it significantly decreased H3K9ac in male *Adnp*^{mut} mice (males, WT + sal: $n = 9$, *Adnp*^{mut} + sal: $n = 8$, *Adnp*^{mut} + LSD1i: $n = 10$, $F_{2,24} = 6.9$, $p = 0.004$, one-way ANOVA).

LSD1 has also been implicated in regulating repressive H3K9 di- or tri-methylation (Metzger et al. 2005), thus, we further examined the effect of GSK-LSD1 on these histone marks in *Adnp*^{mut} mice. As shown in Figure 6B, GSK-LSD1 treatment of female *Adnp*^{mut} mice caused a significant reduction of H3K9me2 and H3K9me3 levels, compared to saline-treated WT or *Adnp*^{mut} female mice (H3K9me2: $F_{2,24} = 18.2$, $p < 0.001$, H3K9me3: $F_{2,24} = 16.3$, $p < 0.001$, one-way ANOVA). In males, H3K9me2 level was significantly lower in saline- or LSD1i-treated *Adnp*^{mut} mice than WT ($F_{2,24} = 5.8$, $p = 0.009$, one-way ANOVA), while H3K9me3 level was similar among all three groups.

Among the presynaptic genes critically involved in synaptic organization or transmitter release, *Nrxn1* (Neurexin 1), *Nrxn3* (Neurexin 3), and *Syp* (Synaptophysin) (Figure 7A), female *Adnp*^{mut} mice showed the reduction of *Nrxn3*, male *Adnp*^{mut} mice exhibited the reduction of *Nrxn1*, and GSK-LSD1 treatment elevated all the three genes in both sexes (*Nrxn1*, females: $F_{2,28} = 4.1$, $p = 0.028$, males: $F_{2,29} = 3.0$, $p = 0.07$; *Nrxn3*, females: $F_{2,28} = 5.6$, $p = 0.009$, males: $F_{2,29} = 4.8$, $p = 0.016$; *Syp*, females: $F_{2,28} = 4.9$, $p = 0.02$, males: $F_{2,18} = 1.17$, $p = 0.3$, one-way ANOVA).

Among the genes encoding AMPAR subunits, *Gria1, Gria2*, and *Gria3* (Figure 7B), female *Adnp*^{mut} mice showed a significant reduction of *Gria1* and *Gria3*, both of which were significantly reversed by GSK-LSD1 treatment, while in male *Adnp*^{mut} mice, the reduced *Gria1* and *Gria3* were not elevated by GSK-LSD1 (*Gria1*, females: $F_{2,29} = 5.0$, $p = 0.014$, males: $F_{2,24} = 3.06$, $p = 0.066$; *Gria3*, females: $F_{2,21} = 8.2$, $p = 0.0023$, males: $F_{2,20} = 5.0$, $p = 0.017$, one-way ANOVA).

Among the GABA-related genes encoding GABA synthesizing enzymes (*Gad1* and *Gad2*) or $GABA_A$ receptor subunit

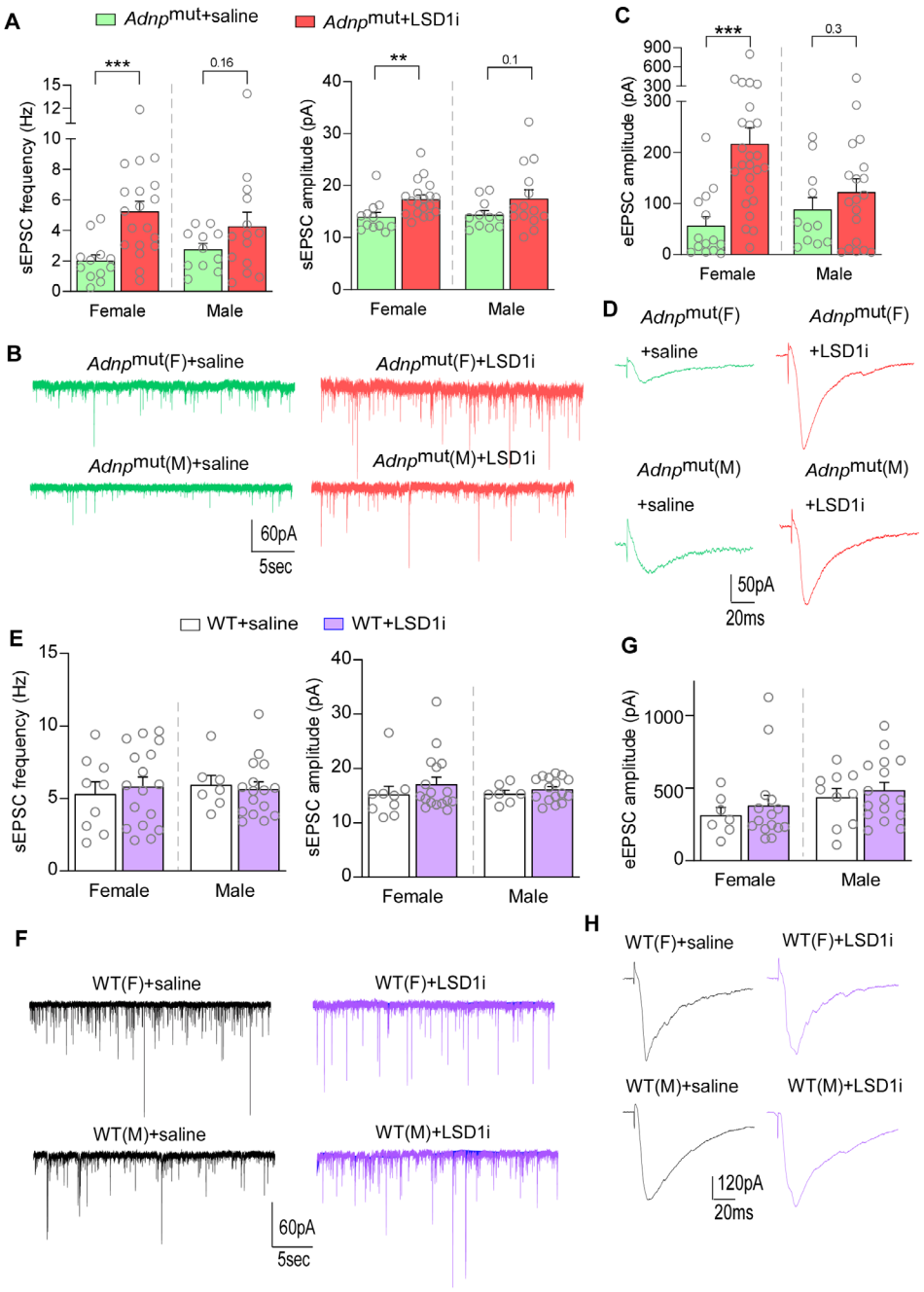

FIGURE 4 | LSD1 inhibitor treatment elevates synaptic excitation in *Adnp*^{mut} mice. (A, C) Bar graphs of sEPSC frequency and amplitude (A) or eEPSC amplitude (C) in PFC pyramidal neurons from female or male *Adnp*^{mut} mice with the treatment of saline vs. GSK-LSD1. (B, D) Representative sEPSC (B) or eEPSC (D) traces. (E–H) Bar graphs of sEPSC frequency and amplitude (E) or eEPSC amplitude (G) in PFC pyramidal neurons from female or male WT mice with the treatment of saline vs. GSK-LSD1. Representative sEPSC and eEPSC traces (F, H) are also shown. All data are shown as mean ± SEM, $^{**}p < 0.01$, $^{***}p < 0.001$, *t* test.

(*Gabrg3*) (Figure 7C), female *Adnp*^{mut} mice had reduced *Gad2* and *Gabrg3*, both of which were significantly increased by GSK-LSD1 treatment (*Gad2*, $F_{2,31} = 4.5$, $p = 0.02$; *Gabrg3*, $F_{2,21} = 8.5$, $p = 0.002$, one-way ANOVA), while no significant changes were found in male *Adnp*^{mut} mice.

These data suggest that the collective changes in synaptic gene expression may lead to the diminished EPSC and IPSC in *Adnp*^{mut} mice, and the restoration or elevation of these synaptic genes by GSK-LSD1 treatment may underlie its rescuing effect on synaptic physiology in *Adnp*^{mut} mice, particularly for females.

4 | Discussion

ADNP, a multifunctional protein, could serve as a chromatin modifier, a translational regulator, an autophagy operator, and a synaptic modulator (Gozes 2016). Although *ADNP* is one of the top ASD risk genes (Satterstrom et al. 2020), the pathophysiological

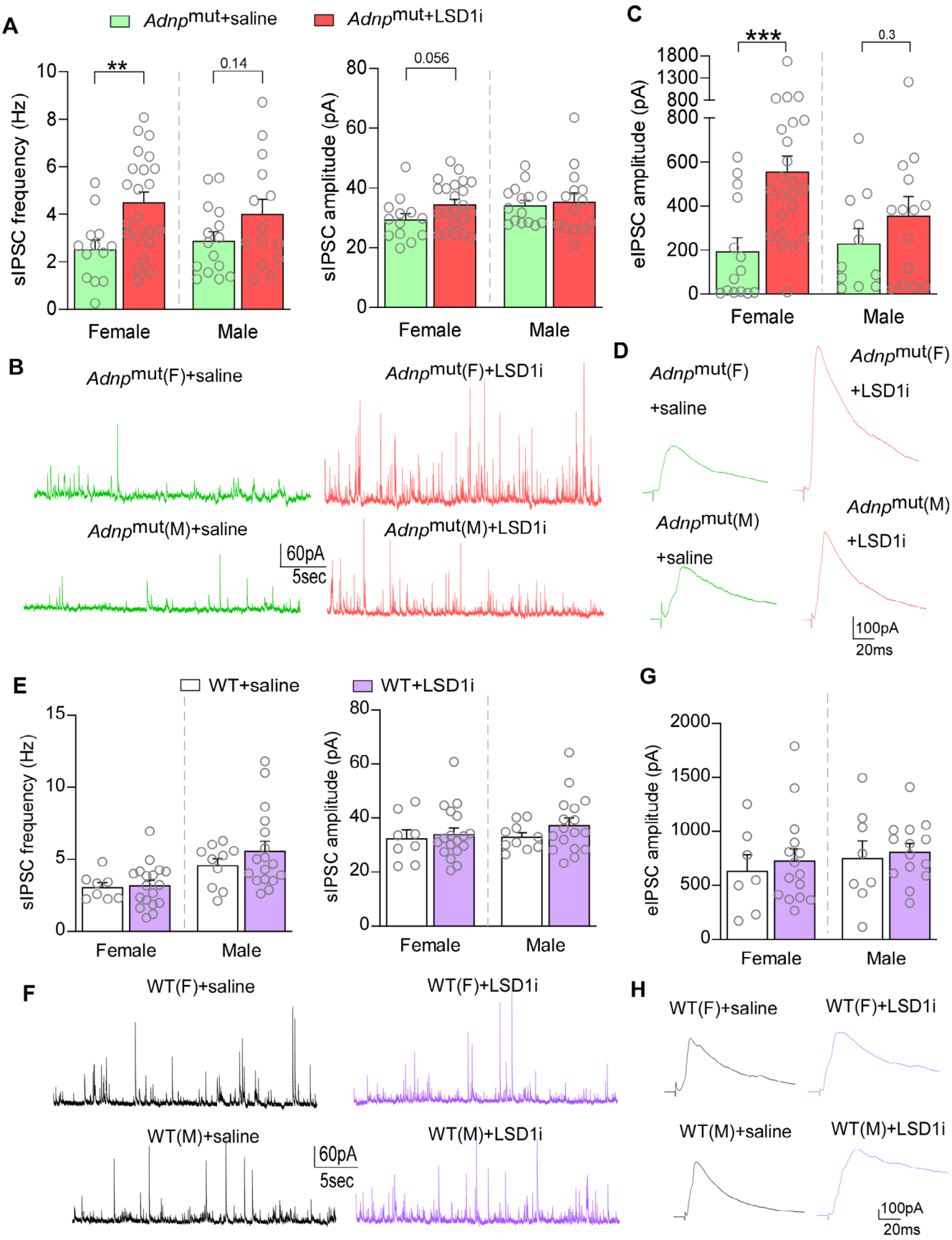

FIGURE 5 | Legend on next page.

FIGURE 5 | LSD1 inhibitor treatment potentiates synaptic inhibition in *Adnp*^{mut} mice. (A, C) Bar graphs of sIPSC frequency and amplitude (A) or eIPSC amplitude (C) in PFC pyramidal neurons from female or male *Adnp*^{mut} mice with the treatment of saline vs. GSK-LSD1. (B, D) Representative sIPSC (B) or eIPSC (D) traces. (E-H) Bar graphs of sIPSC frequency and amplitude (E) or eIPSC amplitude (G) in PFC pyramidal neurons from female or male WT mice with the treatment of saline vs. GSK-LSD1. Representative sIPSC and eIPSC traces (F, H) are also shown. All data are shown as mean ± SEM, $^{**}p < 0.01$, $^{***}p < 0.001$, *t* test.

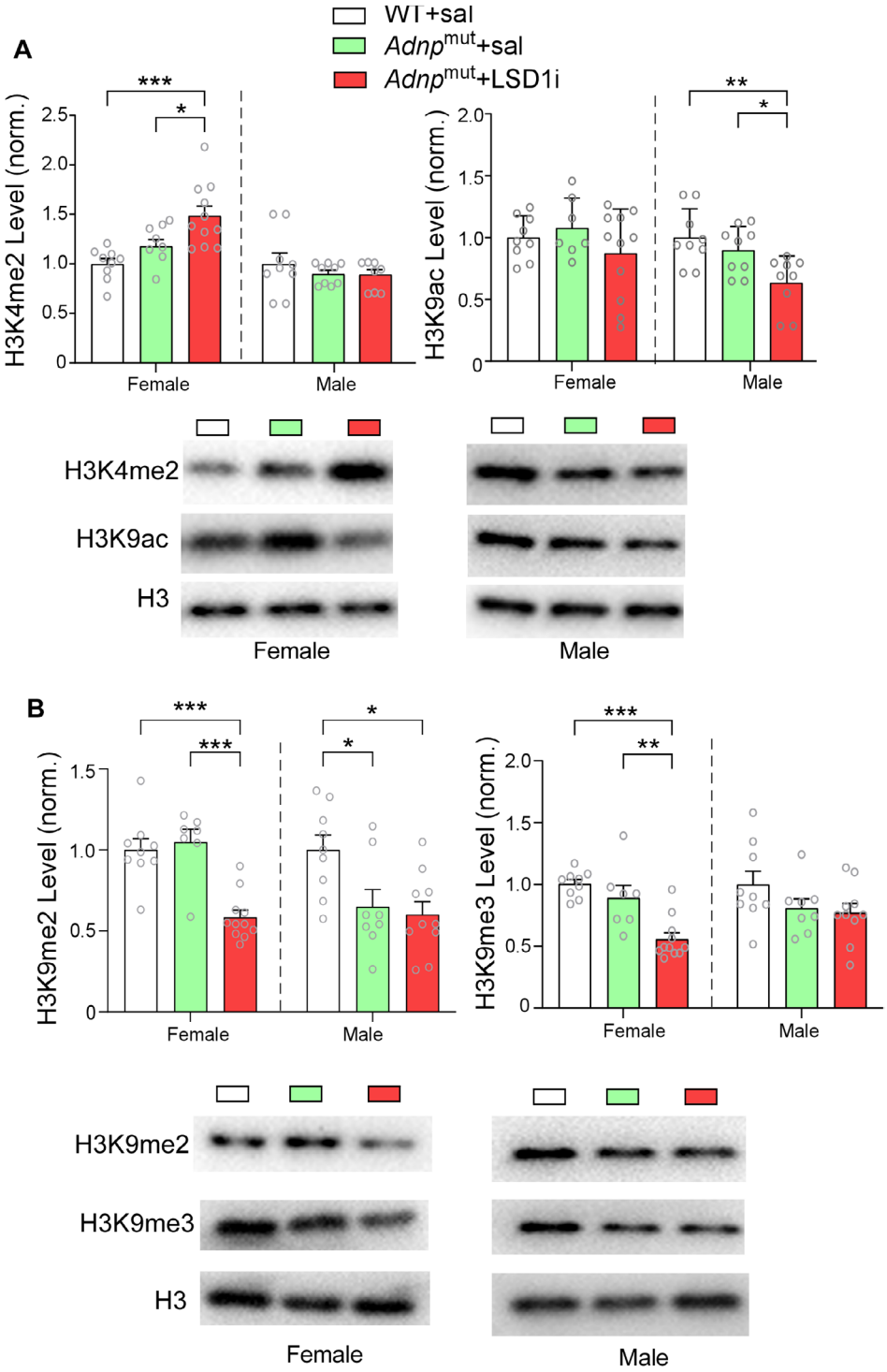

FIGURE 6 | LSD1 inhibitor elevates permissive H3K4me2 and reduces repressive H3K9me2/3 in female *Adnp*^{mut} mice. (A) Bar graphs of immunoblot analysis on histone markers linked to gene activation, H3K4me2 and H3K9ac, in PFC nuclear fraction from female and male WT vs. *Adnp*^{mut} mice treated with saline or GSK-LSD1. Inset: Representative blots. (B) Bar graphs of immunoblot analysis on histone markers linked to gene repression, H3K9me2 and H3K9me3, in PFC nuclear fraction from female and male WT vs. *Adnp*^{mut} mice treated with saline or GSK-LSD1. Inset: Representative blots. All data are shown as mean ± SEM, $^{*}p < 0.05$, $^{**}p < 0.01$, $^{***}p < 0.001$, one-way ANOVA with *post hoc* Tukey's tests.

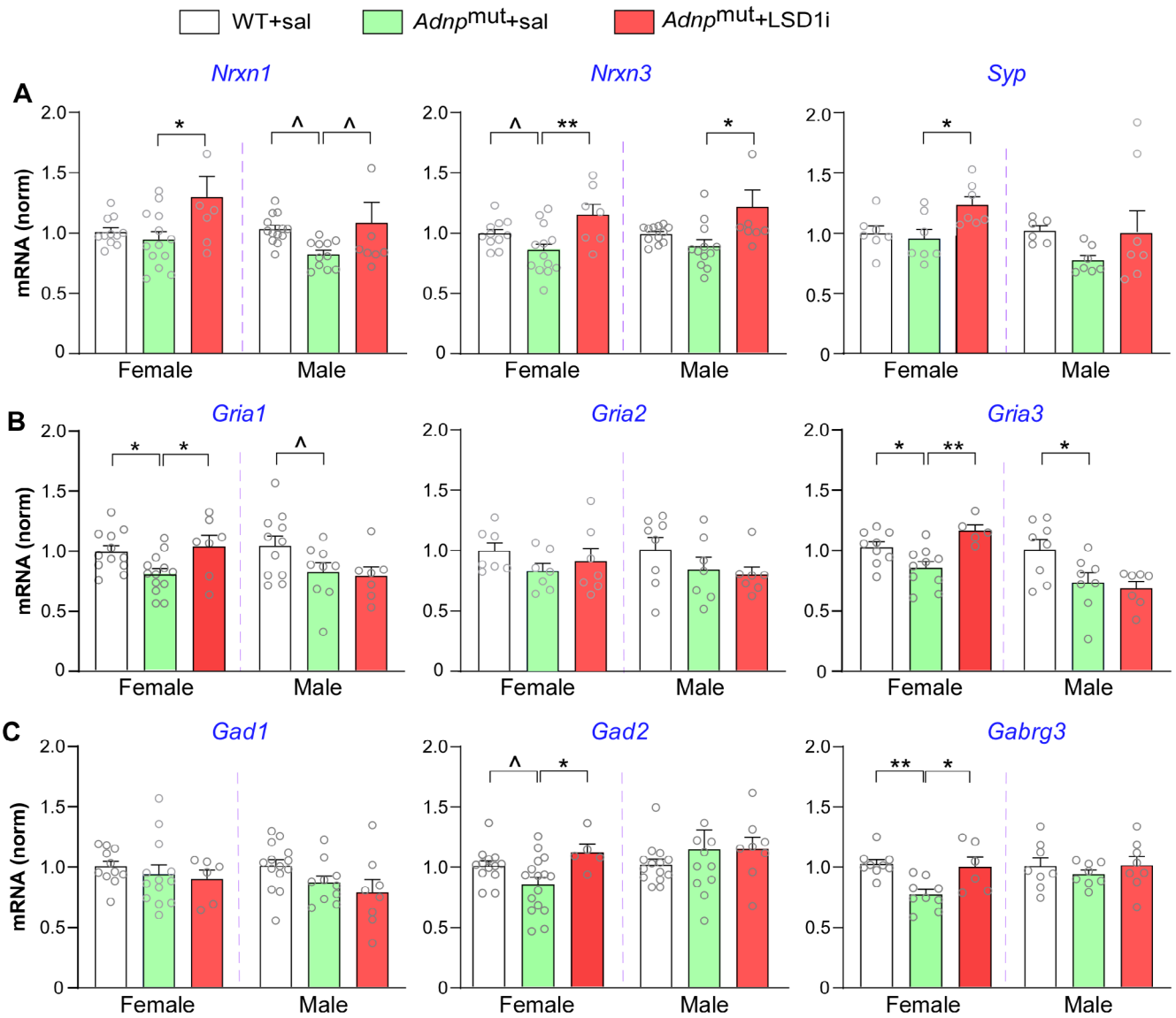

FIGURE 7 | LSD1 inhibitor treatment elevates the expression of diminished synaptic genes in *Adnp*^{mut} mice, especially for females. A–C, Bar graphs of qPCR data showing the mRNA level of synaptic genes in PFC of female or male WT or *Adnp*^{mut} mice with the treatment of saline vs. GSK-LSD1, including presynaptic genes *Nrxn1, Nrxn3* and *Syp* (A), AMPA receptor genes *Gria1, Gria2, and Gria3* (B), and GABA-related genes *Gad1*, *Gad2* and *Gabrg3* (C). All data are shown as mean ± SEM. ^$p < 0.2$, *$p < 0.05$, **$p < 0.01$, ***$p < 0.001$, one-way ANOVA with *post hoc* Tukey's tests.

mechanisms underlying *ADNP* haploinsufficiency-induced ASD are elusive. In this study, we examined the synaptic dysfunction in an *Adnp* mutant mouse model. We found that both excitatory and inhibitory synaptic transmission were significantly diminished in PFC pyramidal neurons of the *Adnp*^{mut} mice. Virus-based knockdown of *Adnp* in PFC of young mice also led to a significant reduction of glutamatergic transmission (Conrow-Graham et al. 2022). In the mouse model with another *Adnp* mutation, synaptic plasticity (LTP/LTD) was altered, while synaptic transmission (EPSC/IPSC) was normal, in adult hippocampal neurons (Cho et al. 2023). It suggests that different *ADNP* mutations may induce diverse synaptic abnormalities in different brain regions.

The alteration of synaptic transmission has been linked to many other top ASD risk genes. For example, *POGZ* deficiency induces the diminished synaptic response mediated by AMPA and NMDA receptors in PFC (Conrow-Graham et al. 2022). *KMT5B* deficiency also leads to PFC glutamatergic hypofunction (Wang et al. 2021). *SHANK3* deficiency specifically impairs NMDAR function in PFC (Duffney et al. 2013, 2015; Qin et al. 2018). *ASH1L* deficiency results in the increased glutamatergic excitation and decreased GABAergic inhibition in PFC, which triggers severe seizures (Qin et al. 2021). *DYRK1A* mutation reduces inhibitory synaptic transmission in hippocampal pyramidal neurons and parvalbumin+ inhibitory neurons (Shih et al. 2023). These data suggest that synaptic aberration is a convergent consequence of the haploinsufficiency of ASD risk genes.

Emerging evidence suggests that a promising therapeutic avenue to rescue synaptic deficits in ASD models is to use pharmacological agents targeting epigenetic enzymes (Yan 2024), such as histone deacetylases (HDAC) (Ma et al. 2018; Qin et al. 2018),

euchromatic histone methyltransferases (EHMT) (Kim et al. 2017; Wang et al. 2020), and lysine-specific histone demethylase 1A (LSD1) (Baba et al. 2021; López-Tobón et al. 2023; Rapanelli et al. 2022). The interaction of LSD1 with ChAHP complex (Barnes et al. 2022) prompted us to examine the therapeutic effects of targeting LSD1 for ADNP mutation-induced synaptic abnormalities. We found that treatment with an LSD1 inhibitor exerted a powerful rescuing effect on glutamatergic and GABAergic synaptic function in *Adnp*^{mut} mice. Consistently, treatment of *Shank3*-deficient autism mouse models with LSD1 inhibitors restored the diminished NMDAR-mediated synaptic currents in PFC pyramidal neurons (Rapanelli et al. 2022). LSD1 inhibitors also normalized dysregulated gene expression in other models for neurodevelopmental disorders (Baba et al. 2021; López-Tobón et al. 2023).

What underlies the therapeutic effects of LSD1 inhibitors? As a histone demethylase, LSD1 could interact with histone H3K4/H3K9/H3K20 to regulate gene expression (Metzger et al. 2005; Perillo et al. 2020; Shi et al. 2004). By probing several histone marks, we found that LSD1 inhibitor elevated the level of H3K4me2 (linked to gene activation) and reduced the level of H3K9me2/3 (linked to gene repression) in female *Adnp*^{mut} mice, which was strongly associated with the elevation or restoration of diminished synaptic genes. These biochemical and molecular data highly corroborate with the electrophysiological data, suggesting that LSD1 inhibitors restore synaptic function in *Adnp*^{mut} mice probably via a histone methylation-dependent mechanism. However, LSD1 may also exert its rescuing effects by interacting with non-histone proteins to regulate transcriptional activation/repression and protein stabilization/degradation (Gu et al. 2020; Maiques-Diaz and Somervaille 2016; Perillo et al. 2020), which awaits to be further investigated.

Between *Adnp*^{mut} and WT mice, we did not find significant differences in the level of four tested histone marks. One possibility is that the electrophysiological and synaptic gene abnormalities in *Adnp*^{mut} mice arise from other histone modifications or independently of histone modifications. Another possibility is that the changes in histone modification may not be global but locus-specific. Even though different mechanisms may underlie the effects of *Adnp* mutation and LSD1 inhibition, they converge on the same targets (synaptic genes and function) in opposite directions.

One interesting finding is that the rescuing effects of the LSD1 inhibitor are more prominent in female *Adnp*^{mut} mice. Sex-specific changes in gene expression, spine density, and behavioral phenotypes induced by *Adnp* mutations have been previously reported (Amal 2022; Gozes 2017; Karmon et al. 2022; Malishkevich et al. 2015). The reason why the LSD1 inhibitor has more pronounced effects on histone marks and synaptic genes/functions in females could be related to the upstream regulators of LSD1 that direct H3K9 or H3K4 demethylation (Kozub et al. 2017). It has been found that the activity of sex hormone (estrogen and androgen) receptors facilitates LSD1 demethylation of H3K9, whereas HDAC1/2 and CoREST promote LSD1 demethylation of H3K4 (Kozub et al. 2017). Besides LSD1, other estrogen-responsive H3K9 demethylases, such as KDM3A (Wade et al. 2015) and KDM4B (Shi et al. 2011), which are particularly elevated in females, could also affect the overall level of H3K9 demethylation.

LSD1 inhibitors have been employed widely in clinical trials for cancer (Agboyibor et al. 2021; Cai et al. 2024; Fang et al. 2019; Højfeldt et al. 2013; Liu et al. 2024), but they were rarely tested for brain disorders (Lacivita et al. 2017; Liu et al. 2024). Since ASD and cancer share many risk genes and pathways (Crawley et al. 2016; Gabrielli et al. 2019; Pedini et al. 2023), they may also share some intervention avenues. The current and prior preclinical studies have uncovered the therapeutic potential of LSD1 inhibitors for ASD (Baba et al. 2021; López-Tobón et al. 2023; Rapanelli et al. 2022), providing the basis for developing clinical trials using LSD1 inhibitors for neurodevelopmental disorders.

Author Contributions

C.-H.L. performed electrophysiological experiments, analyzed data, and wrote the draft. Y.R. performed qPCR experiments and analyzed data. K.W.T. performed Western blotting experiments and analyzed data. M.C.-G. characterized the mutant mice. Z.Y. designed experiments, supervised the project, and wrote the paper.

Acknowledgments

We thank Xiaoqing Chen and Rachel Senek for their excellent technical support.

Conflicts of Interest

The authors declare no conflicts of interest.

Data Availability Statement

The data that support the findings of this study are available on request from the corresponding author.

References

Agboyibor, C., J. Dong, C. Y. Effah, E. K. Drokow, W. Pervaiz, and H.-M. Liu. 2021. "LSD1 as a Biomarker and the Outcome of Its Inhibitors in the Clinical Trial: The Therapy Opportunity in Tumor." *Journal of Oncology* 2021: 5512524.

Amal, H. 2022. "Sex and the Brain: Novel ADNP Syndrome Mice Are Protected by NAP." *Biological Psychiatry* 92: 8–9.

Baba, R., S. Matsuda, Y. Arakawa, et al. 2021. "LSD1 Enzyme Inhibitor TAK-418 Unlocks Aberrant Epigenetic Machinery and Improves Autism Symptoms in Neurodevelopmental Disorder Models." *Science Advances* 7: eaba1187.

Barnes, C. E., D. M. English, M. Broderick, M. O. Collins, and S. M. Cowley. 2022. "Proximity-Dependent Biotin Identification (BioID) Reveals a Dynamic LSD1–CoREST Interactome During Embryonic Stem Cell Differentiation." *Molecular Omics* 18: 31–44.

Bassan, M., R. Zamostiano, A. Davidson, et al. 1999. "Complete Sequence of a Novel Protein Containing a Femtomolar-Activity-Dependent Neuroprotective Peptide." *Journal of Neurochemistry* 72: 1283–1293.

Cai, W., C. Xiao, T. Fan, et al. 2024. "Targeting LSD1 in Cancer: Molecular Elucidation and Recent Advances." *Cancer Letters* 598: 217093.

Cho, H., T. Yoo, H. Moon, et al. 2023. "Adnp-Mutant Mice With Cognitive Inflexibility, CaMKIIα Hyperactivity, and Synaptic Plasticity Deficits." *Molecular Psychiatry* 28: 3548–3562.

Conrow-Graham, M., J. B. Williams, J. Martin, et al. 2022. "A Convergent Mechanism of High Risk Factors ADNP and POGZ in Neurodevelopmental Disorders." *Brain* 145: 3250–3263.

Crawley, J. N., W.-D. Heyer, and J. M. LaSalle. 2016. "Autism and Cancer Share Risk Genes, Pathways, and Drug Targets." *Trends in Genetics* 32: 139–146.

De Rubeis, S., X. He, A. P. Goldberg, et al. 2014. "Synaptic, Transcriptional and Chromatin Genes Disrupted in Autism." *Nature* 515: 209–215.

Delorme, R., E. Ey, R. Toro, M. Leboyer, C. Gillberg, and T. Bourgeron. 2013. "Progress Toward Treatments for Synaptic Defects in Autism." *Nature Medicine* 19: 685–694.

D'Incal, C. P., K. E. Van Rossem, K. De Man, et al. 2023. "Chromatin Remodeler Activity-Dependent Neuroprotective Protein (ADNP) Contributes to Syndromic Autism." *Clinical Epigenetics* 15: 45.

Duffney, L. J., J. Wei, J. Cheng, et al. 2013. "Shank3 Deficiency Induces NMDA Receptor Hypofunction via an Actin-Dependent Mechanism." *Journal of Neuroscience* 33: 15767–15778.

Duffney, L. J., P. Zhong, J. Wei, et al. 2015. "Autism-Like Deficits in Shank3-Deficient Mice Are Rescued by Targeting Actin Regulators." *Cell Reports* 11: 1400–1413.

Fang, Y., G. Liao, and B. Yu. 2019. "LSD1/KDM1A Inhibitors in Clinical Trials: Advances and Prospects." *Journal of Hematology & Oncology* 12: 129.

Gabrielli, A. P., A. M. Manzardo, and M. G. Butler. 2019. "GeneAnalytics Pathways and Profiling of Shared Autism and Cancer Genes." *International Journal of Molecular Sciences* 20: 1166.

Gozes, I. 2016. "The Cytoskeleton as a Drug Target for Neuroprotection: The Case of the Autism-Mutated ADNP." *Biological Chemistry* 397: 177–184.

Gozes, I. 2017. "Sexual Divergence in Activity-Dependent Neuroprotective Protein Impacting Autism, Schizophrenia, and A Lzheimer's Disease." *Journal of Neuroscience Research* 95: 652–660.

Gu, F., Y. Lin, Z. Wang, et al. 2020. "Biological Roles of LSD1 Beyond Its Demethylase Activity." *Cellular and Molecular Life Sciences* 77: 3341–3350.

Hacohen-Kleiman, G., S. Sragovich, G. Karmon, et al. 2018. "Activity-Dependent Neuroprotective Protein Deficiency Models Synaptic and Developmental Phenotypes of Autism-Like Syndrome." *Journal of Clinical Investigation* 128: 4956–4969.

Helsmoortel, C., A. T. Vulto-van Silfhout, B. P. Coe, et al. 2014. "A SWI/SNF-Related Autism Syndrome Caused by de Novo Mutations in ADNP." *Nature Genetics* 46: 380–384.

Højfeldt, J. W., K. Agger, and K. Helin. 2013. "Histone Lysine Demethylases as Targets for Anticancer Therapy." *Nature Reviews Drug Discovery* 12: 917–930.

Kaaij, L. J. T., F. Mohn, R. H. van der Weide, E. de Wit, and M. Bühler. 2019. "The ChAHP Complex Counteracts Chromatin Looping at CTCF Sites That Emerged From SINE Expansions in Mouse." *Cell* 178: 1437–51.e14.

Karmon, G., S. Sragovich, G. Hacohen-Kleiman, et al. 2022. "Novel ADNP Syndrome Mice Reveal Dramatic Sex-Specific Peripheral Gene Expression With Brain Synaptic and Tau Pathologies." *Biological Psychiatry* 92: 81–95.

Kim, Y., H.-M. Lee, Y. Xiong, et al. 2017. "Targeting the Histone Methyltransferase G9a Activates Imprinted Genes and Improves Survival of a Mouse Model of Prader–Willi Syndrome." *Nature Medicine* 23: 213–222.

Kozub, M. M., R. M. Carr, G. L. Lomberk, and M. E. Fernandez-Zapico. 2017. "LSD1, a Double-Edged Sword, Confers Dynamic Chromatin Regulation but Commonly Promotes Aberrant Cell Growth." *F1000Res* 6: 2016.

Lacivita, E., R. Perrone, L. Margari, and M. Leopoldo. 2017. "Targets for Drug Therapy for Autism Spectrum Disorder: Challenges and Future Directions." *Journal of Medicinal Chemistry* 60: 9114–9141.

Liu, H. M., Y. Zhou, H. X. Chen, et al. 2024. "LSD1 in Drug Discovery: From Biological Function to Clinical Application." *Medicinal Research Reviews* 44: 833–866.

Longaretti, A., C. Forastieri, E. Toffolo, et al. 2020. "LSD1 Is an Environmental Stress-Sensitive Negative Modulator of the Glutamatergic Synapse." *Neurobiology of Stress* 13: 100280.

López-Tobón, A., R. Shyti, C. E. Villa, et al. 2023. "GTF2I Dosage Regulates Neuronal Differentiation and Social Behavior in 7q11.23 Neurodevelopmental Disorders." *Science Advances* 9: eadh2726.

Ma, K., L. Qin, E. Matas, L. J. Duffney, A. Liu, and Z. Yan. 2018. "Histone Deacetylase Inhibitor MS-275 Restores Social and Synaptic Function in a Shank3-Deficient Mouse Model of Autism." *Neuropsychopharmacology* 43: 1779–1788.

Maiques-Diaz, A., and T. C. Somervaille. 2016. "LSD1: Biologic Roles and Therapeutic Targeting." *Epigenomics* 8: 1103–1116.

Malishkevich, A., N. Amram, G. Hacohen-Kleiman, I. Magen, E. Giladi, and I. Gozes. 2015. "Activity-Dependent Neuroprotective Protein (ADNP) Exhibits Striking Sexual Dichotomy Impacting on Autistic and Alzheimer's Pathologies." *Translational Psychiatry* 5: e501–e501.

Mandel, S., and I. Gozes. 2007. "Activity-Dependent Neuroprotective Protein Constitutes a Novel Element in the SWI/SNF Chromatin Remodeling Complex." *Journal of Biological Chemistry* 282: 34448–34456.

Markenscoff-Papadimitriou, E., F. Binyameen, S. Whalen, et al. 2021. "Autism Risk Gene POGZ Promotes Chromatin Accessibility and Expression of Clustered Synaptic Genes." *Cell Reports* 37: 110089.

Metzger, E., M. Wissmann, N. Yin, et al. 2005. "LSD1 Demethylates Repressive Histone Marks to Promote Androgen-Receptor-Dependent Transcription." *Nature* 437: 436–439.

Mukai, J., E. Cannavò, G. W. Crabtree, et al. 2019. "Recapitulation and Reversal of Schizophrenia-Related Phenotypes in Setd1a-Deficient Mice." *Neuron* 104: 471–87. e12.

Ostapcuk, V., F. Mohn, S. H. Carl, et al. 2018. "Activity-Dependent Neuroprotective Protein Recruits HP1 and CHD4 to Control Lineage-Specifying Genes." *Nature* 557: 739–743.

Oz, S., O. Kapitansky, Y. Ivashco-Pachima, et al. 2014. "The NAP Motif of Activity-Dependent Neuroprotective Protein (ADNP) Regulates Dendritic Spines Through Microtubule End Binding Proteins." *Molecular Psychiatry* 19: 1115–1124.

Pedini, G., C.-L. Chen, T. Achsel, and C. Bagni. 2023. "Cancer Drug Repurposing in Autism Spectrum Disorder." *Trends in Pharmacological Sciences* 44: 963–977.

Perillo, B., A. Tramontano, A. Pezone, and A. Migliaccio. 2020. "LSD1: More Than Demethylation of Histone Lysine Residues." *Experimental & Molecular Medicine* 52: 1936–1947.

Qin, L., K. Ma, Z.-J. Wang, et al. 2018. "Social Deficits in Shank3-Deficient Mouse Models of Autism Are Rescued by Histone Deacetylase (HDAC) Inhibition." *Nature Neuroscience* 21: 564–575.

Qin, L., J. B. Williams, T. Tan, et al. 2021. "Deficiency of Autism Risk Factor ASH1L in Prefrontal Cortex Induces Epigenetic Aberrations and Seizures." *Nature Communications* 12: 6589.

Rapanelli, M., J. B. Williams, K. Ma, et al. 2022. "Targeting Histone Demethylase LSD1 for Treatment of Deficits in Autism Mouse Models." *Molecular Psychiatry* 27: 3355–3366.

Satterstrom, F. K., J. A. Kosmicki, J. Wang, et al. 2020. "Large-Scale Exome Sequencing Study Implicates Both Developmental and Functional Changes in the Neurobiology of Autism." *Cell* 180: 568–84.e23.

Shi, Y., F. Lan, C. Matson, et al. 2004. "Histone Demethylation Mediated by the Nuclear Amine Oxidase Homolog LSD1." *Cell* 119: 941–953.

Shi, L., L. Sun, Q. Li, et al. 2011. "Histone Demethylase JMJD2B Coordinates H3K4/H3K9 Methylation and Promotes Hormonally Responsive Breast Carcinogenesis." *Proceedings of the National Academy of Sciences of the United States of America* 108: 7541–7546.

Shih, Y.-T., J. B. Alipio, and A. Sahay. 2023. "An Inhibitory Circuit-Based Enhancer of Dyrk1a Function Reverses Dyrk1a-Associated Impairment in Social Recognition." *Neuron* 111: 3084–101. e5.

Spooren, W., L. Lindemann, A. Ghosh, and L. Santarelli. 2012. "Synapse Dysfunction in Autism: A Molecular Medicine Approach to Drug Discovery in Neurodevelopmental Disorders." *Trends in Pharmacological Sciences* 33: 669–684.

Sun, X., W. Yu, L. Li, and Y. Sun. 2020. "ADNP Controls Gene Expression Through Local Chromatin Architecture by Association With BRG1 and CHD4." *Frontiers in Cell and Developmental Biology* 8: 553.

Van Dijck, A., A. T. Vulto-van Silfhout, E. Cappuyns, et al. 2019. "Clinical Presentation of a Complex Neurodevelopmental Disorder Caused by Mutations in ADNP." *Biological Psychiatry* 85: 287–297.

Wade, M. A., D. Jones, L. Wilson, et al. 2015. "The Histone Demethylase Enzyme KDM3A Is a Key Estrogen Receptor Regulator in Breast Cancer." *Nucleic Acids Research* 43: 196–207.

Wan, L., G. Yang, and Z. Yan. 2024. "Identification of a Molecular Network Regulated by Multiple ASD High Risk Genes." *Human Molecular Genetics* 33: 1176–1185.

Wang, Z.-J., B. Rein, P. Zhong, et al. 2021. "Autism Risk Gene KMT5B Deficiency in Prefrontal Cortex Induces Synaptic Dysfunction and Social Deficits via Alterations of DNA Repair and Gene Transcription." *Neuropsychopharmacology* 46: 1617–1626.

Wang, Z.-J., P. Zhong, K. Ma, et al. 2020. "Amelioration of Autism-Like Social Deficits by Targeting Histone Methyltransferases EHMT1/2 in Shank3-Deficient Mice." *Molecular Psychiatry* 25: 2517–2533.

Yan, Z. 2024. "Targeting Epigenetic Enzymes for Autism Treatment." *Trends in Pharmacological Sciences* 45: 764–767.

Yan, Z., and B. Rein. 2022. "Mechanisms of Synaptic Transmission Dysregulation in the Prefrontal Cortex: Pathophysiological Implications." *Molecular Psychiatry* 27: 445–465.